

Supplementary Material: Low meteorological influence found in 2019 Amazonia fires

Douglas I. Kelley^{1*}, Chantelle Burton², Chris Huntingford¹, Megan A. J. Brown^{1,3}, Rhys Whitley⁴, Ning Dong⁵

¹ UK Centre for Ecology & Hydrology, Wallingford, Oxfordshire, OX10 8BB, U.K.

² Met Office Hadley Centre, Fitzroy Road, Exeter. EX1 3PB

³ School of Physical Sciences, The Open University, Walton Hall, Milton Keynes, MK7 6AA, UK

⁴ Natural Perils Pricing, Commercial and Consumer Portfolio and Product, Suncorp Group, Sydney, Australia

⁵ Department of Biological Sciences, Macquarie University, North Ryde, NSW 2109, Australia

10 *Correspondence to:* Douglas I. Kelley (douglas.i.kelley@gmail.com)

Model Evaluation

We used the same set of evaluation as Kelley et al. (2019). As we are also looking at annual variations for seasonal and sub-seasonal model simulation of burnt area, we also included additional comparisons for seasonal and interannual variability. Comparisons were made against MCD64A1 for 15 July 2002 - June 2018. Monthly gridded simulations for all 1000 posterior samples were compared using Normalised Mean Squared Error (*NMSE*) (Kelley et al., 2013). Annual average and June to September average comparisons used Normalised Mean Error (*NME*) (Kelley et al., 2013) as recommended by the Fire Model Intercomparison Project (FireMIP, (Rabin et al., 2017)). *NMSE* and *NME* sum the squared (for *NMSE*) or absolute (for *NME*) distance between observations (*obs*) and 20 reconstructed burnt area from a parameter set (*sim*(β)) over all cells (*i*) weighted by cell area (A_i) and normalised by mean variation in *obs*:

$$NME = \frac{\sum_i A_i \times |sim(\beta_i) - obs_i|}{\sum_i A_i \times |obs - obs_i|} \quad \text{and} \quad NMSE = \frac{\sum_i A_i \times (sim(\beta_i) - obs_i)^2}{\sum_i A_i \times (obs - obs_i)^2} \quad (S1)$$

NME and *NMSE* comparisons were conducted in three steps:

1. As described above;
- 25 2. Comparing obs_i and sim_i after taking the difference between their respective means, thereby removing systematic bias
3. obs_i and sim_i are additionally divided by the mean deviation, which therefore describes the models' ability to reproduce the spatial pattern in burnt area.

Seasonality comparisons were conducted in three parts: 1) modality - i.e how many “seasons” there
 30 are in a given year; 2) phase, or timing, of the season; and 3) seasonal concentration (inverse of
 season length).

To determine the modality of a given cell, we first calculated the monthly climatology (v_0). The month
 of the minimum burnt area from this climatology was defined as the start of the “fire year”. We then
 found the position (P) of each maxima turning point (p_i) throughout the year:

$$35 \quad v(1) = \min(v_0)$$

$$P = \left\{ p_i \mid \frac{dv(p_i)}{dt} = 0 \wedge \frac{d^2v(p_i)}{dt^2} < 0 \wedge v(p_i) < v(p_{i+1}) \right\} \quad (S2)$$

The modality (MOD) was then the prominence of each of these turning points (i.e the minimum drop
 required to the next turning point), weighted by the phase distance (θ) to the next turning point. This
 40 is normalised by the height of the month of maximum burnt area

$$\theta_p = 2 \times \pi \times (p - 1) / 12 \quad (S3)$$

$$MOD = 1 + \frac{\sum_{i=1}^{p-1} (v(p_i) - \min\{v(p_i), v(p_{i+1})\}) \times (1 - \cos(\theta_{p_i} - \theta_{p_{i+1}}))}{2 \times (max(v) - v(1))} \quad (S4)$$

If there was no fire, then MOD is undefined and no comparison was made for that grid cell. If there
 were no turning points, then modality was set to 0. If there was one turning point, MOD was set to 1.
 45 The higher the number beyond that, the higher the modality the more “seasons” within a year. Two
 equally prominent peaks 6 months apart have a modality of 2. Observational and simulated MOD was
 then compared using NME .

Phase and concentration comparisons were conducted as per (Kelley et al., 2013), each month, p , is
 represented by a vector whose direction corresponds to the time of year (equation S3) and length to
 50 the magnitude of the variable for that month. A mean vector L was calculated by averaging the x (L_x)
 and y (L_y) components of the 12 vectors (x_p).

$$\begin{aligned} L_x &= \sum_p x_p \times \cos(\theta_p) \\ L_y &= \sum_p x_p \times \sin(\theta_p) \end{aligned} \quad (S5)$$

The mean vector length by the annual average described the seasonal concentration (C) of burnt area, whilst it's direction (P) described season timing:

$$C = \frac{\sqrt{L_x^2 + L_y^2}}{\sum p x_p} \quad (S6)$$

$$P = \arctan(L_x/L_y) \quad (S7)$$

60

If burnt area in a given cell was concentrated all in one month, C was equal to 1 and P corresponded to that month. If burnt area was evenly spread throughout the year then concentration was set to zero and phase undefined and was not used in the comparison. Likewise, if a cell had zero annual average burnt area for either observations or simulation, then that cell was not included in the comparisons.

65 Concentration was compared using NME step 1. Phases were compared using mean phase difference (MPD)

$$MPD = \frac{1}{\pi} \cdot \sum_i A_i \cdot \arccos \left[\cos \left(P_{sim,i} - P_{obs,i} \right) \right] / \sum_i A_i \quad (S8)$$

70 MPD represents the average timing error, as a proportion of the maximum phase mismatch (6 months).

We assessed temporal variations using spearman's rank (Dodge, 2008; Lasslop et al., 2018). This was performed for each grid cell both monthly and, to assess inter-annual variability, annually-averaged burnt area. The score was then the area-weighted average comparison of all grid cells.

75 Smaller NME , $NMSE$ and MPD scores indicate a better agreement between simulation and observation, with a perfect score (i.e., simulation that perfectly matches observations) of 0. Greater spearman's rank scores indicate better performance, with a score of 1 occurring with perfect ordering in the simulation and -1 complete reverse ordering. We also used three null models to help interpret the score as per (Burton et al., 2019; Kelley et al., 2019). The mean null model compared the mean of
80 all observations with the observations. For NME and $NMSE$, the mean null model was always 1 as these metrics are normalised by the mean difference. As there is no ordering in a mean null model, the spearman's rank comparison gives a score of 0. The best "single value" model compared the median of observations to observations. By definition, it's score is less than or equal to the mean model score for NME and, again, a score of 0 for spearman's rank. The mean and median null model scores for
85 MPD depends on the observations. The "randomly resampled" null model compared randomly-resampled observations (without replacement) to the observations. The score depends on the resampling order, so we used 1000 bootstraps to determine the null models' distribution.

Our monthly *NMSE* step 1 scores of 0.678-0.693 (based on 5-95% percentile, Fig. S1) are much better than all null models. *NMSE* is proportional to our error term in equation 3, indicating good
90 convergence of the model, though the Fig. 1 time series demonstrates that a lot of the models' posterior spread is still within the error term rather than parameter uncertainty, suggesting that further development of the models' process representation is still possible (see discussion).

Our reconstructed annual average burnt area *NME* step 1 scores of 0.606-0.616 is comparable to the comparison between training observations and simulation in the global model, which obtained scores
95 of 0.603-0.630 (Kelley et al., 2019). Our conversion to a coarser grid and pragmatic choice of variables have therefore not been detrimental for model performance, possibly helped by our restricted geographic range. Step 3 scores of 0.680-0.691, are 17-19% better than our best null model which suggests good performance in the spatial pattern of burnt areas. The model spatial burnt area is even better for the fire season (Fig. 2 and 3), with step 1 scores of 0.468-0.485 and step 3 of
100 0.532-0.548. However, the median null model also improves, which suggests that capturing the fire season should be easier, though it should be noted that other fire models normally struggle to pick up high burnt areas during fire season peaks (Hantson et al., 2020).

The model largely identifies regions with bimodal fire seasons (Fig. S2), though with 33.6% of the posteriors Step 3 scores being greater than the mean null model suggests that this is not easily
105 captured by the model. Seasonal human fire manipulation is often a cause of bimodal fire systems (Archibald et al., 2009; Hall et al., 2016), which is not included in the modelling framework and again would be useful in future studies (see discussion). For single modal systems, the timing of the fire season is very well captured in the model (Fig. S3), with a score of 0.153-0.164, 48-52% better than the closest null model. Most (58.1) seasonal concentrations of the model are better than the mean null
110 model. However, the fire season is often too short in agricultural areas (Fig. S2). Again, this could be due to the lack of seasonal variation in human fire starts (Archibald et al., 2009; Hall et al., 2016).

Overall, the model correctly ranks the months' burnt area (Fig. S1 and S2) with a score of 0.497-0.543, demonstrating that the overall season is well represented. The model also correctly ranks the ordering of annual burnt areas (Fig. S3), scoring 0.227-0.236 - better than all null models, thereby
115 showing that it is able to capture the interannual variability. For our AAD region, these improve further, with 0.703-0.724 for monthly ranking and 0.412-0.422 for annual ranking (Fig. S1).

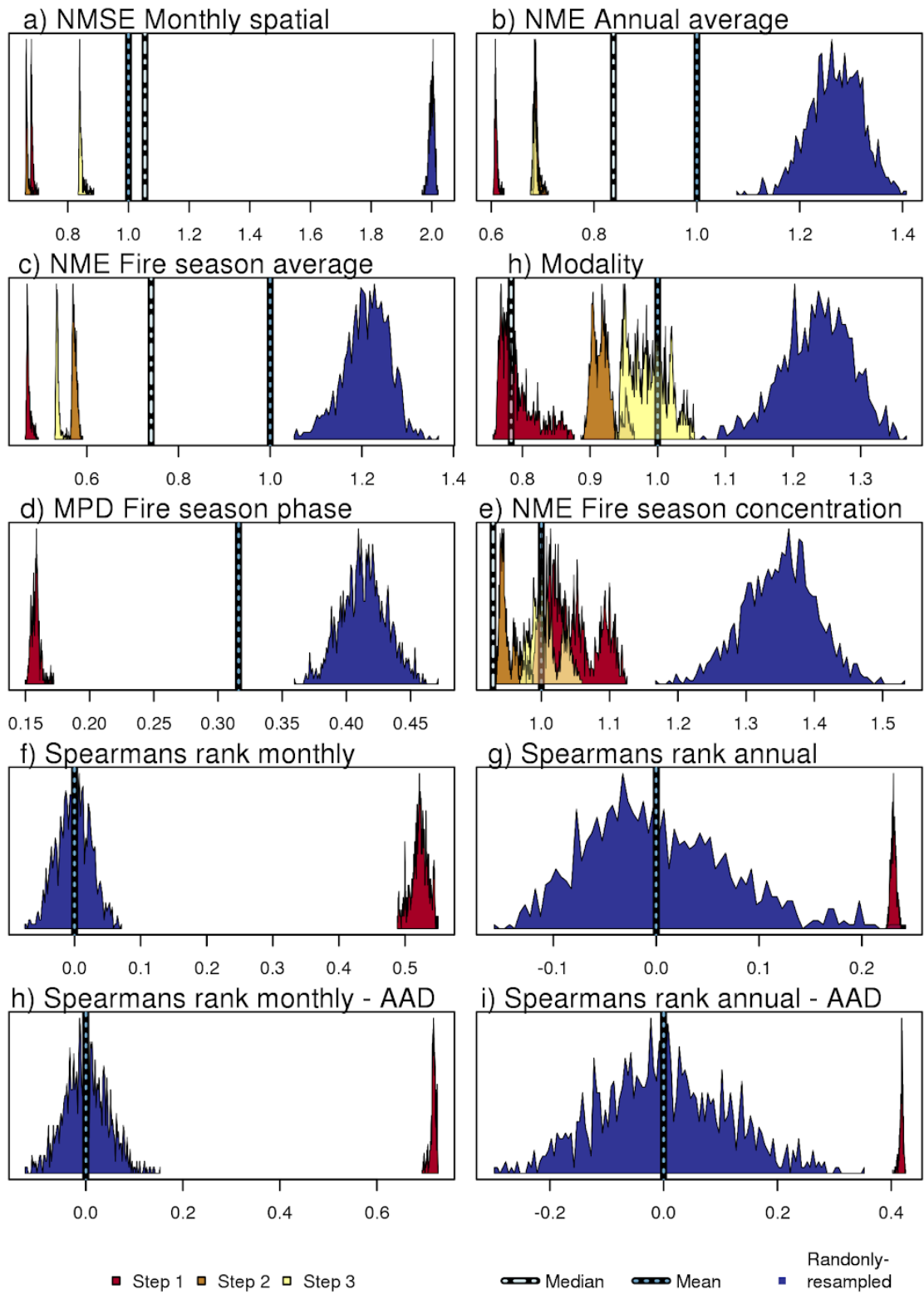


Figure S1: Metric scores for the models posterior for steps 1-3 (red, orange and yellow) and median (grey dot-dashed line), mean (light blue dashed) and randomly-resampled (blue distribution) null models.

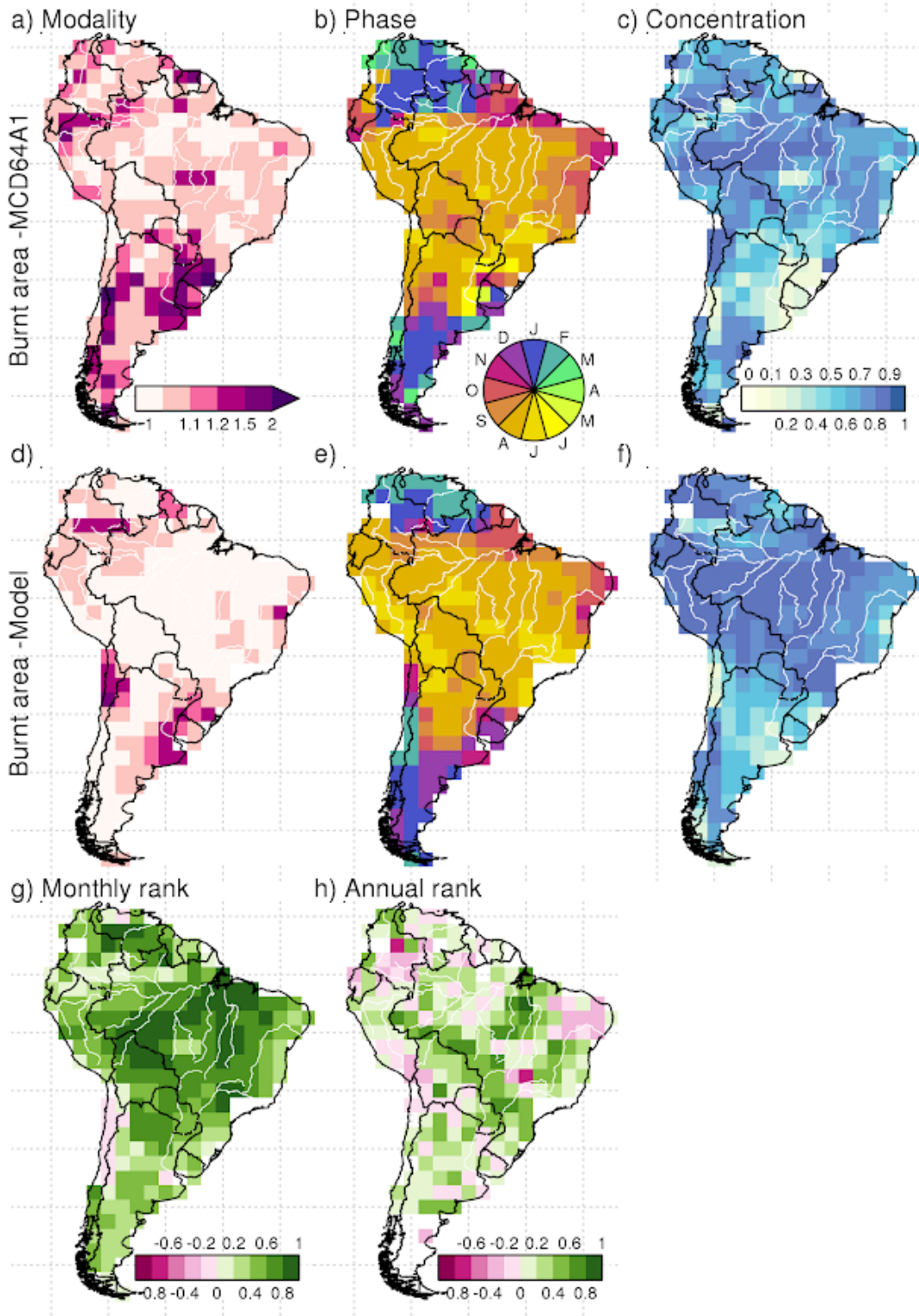


Figure S2: Seasonal comparisons for (top row) MCD64A1 observed and (2nd row) 50% percentile of the models posterior for (1st column) modality, (2nd column) phase of the timing of the fire season and (3rd column) concentration (inverse of season length) of the fire season. The bottom row shows the spatial pattern of spearman's rank comparisons between MCD64A1 and the 50% percentile of the models posterior and a monthly and annual timestep.

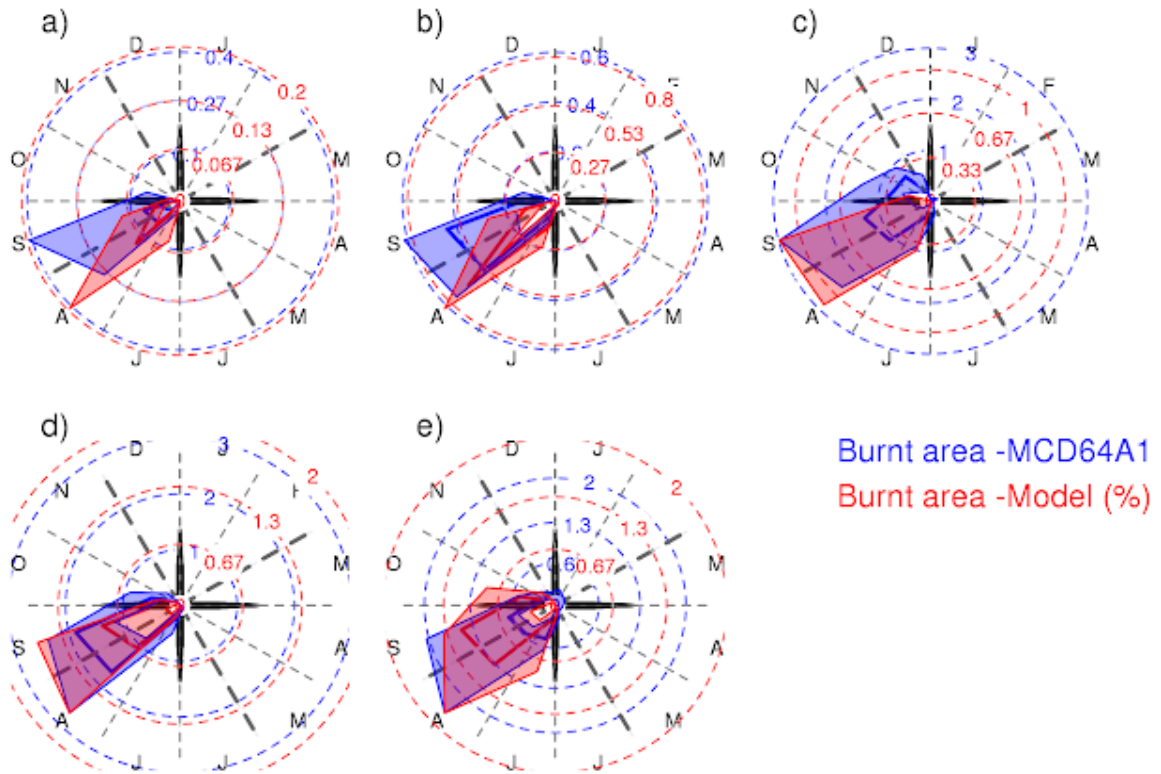


Figure S3: 2002-2018 climatology for MCD64A1 observed burnt area on the 50% percentile model for each region. The thick line shows the median of all cells in the region, while shaded areas show full range.

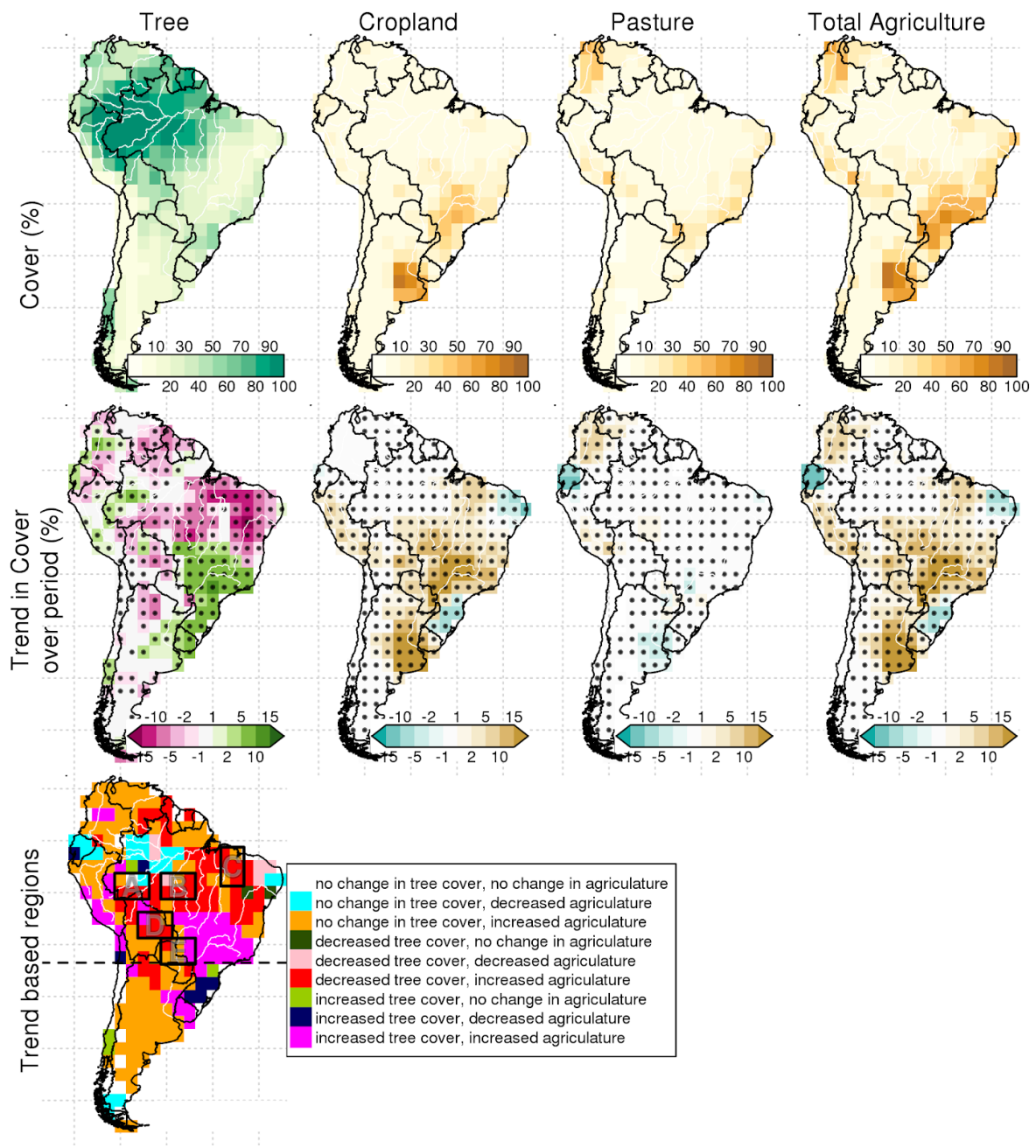


Figure S4: Changes in tree cover and agriculture from 2002-2018. Top row shows (from left to right) percentage tree cover from VCF (Dimiceli et al., 2015), and cropland, pasture and total agricultural cover from HYDEv3.1 (Klein Goldewijk et al., 2010). The 2nd row shows the corresponding trends in tree cover and agriculture in percentage over 2002-2018. As variables are bounded, we use the trend analysis from (Kelley et al., 2019) using the “greenbrown” R package (Forkel et al., 2013, 2015). Dots signify areas of significant trends (p-value < 0.05). The bottom map shows areas of increases, decreases or no significant trend in tree cover and agriculture. Red areas indicate our “area of active deforestation” (F in Fig. 1).

Table S1: Controls, drivers and target variables and data sources used in the model

Control	Variable	Calculated as	Data source
Fuel continuity “Fuel” (%)	Total vegetation cover (%)	1 - bare cover	MODIS Vegetation Continuous Fields (VCF) (Dimiceli et al., 2015)
	Maximum seasonal anomalies in water availability	$\frac{\theta}{\theta_{mean}} - 1$ (see row below)	NCEP/NCAR soil moisture (Kalnay et al., 1996)
Fuel moisture “Moisture” (%)	Soil moisture (%) - θ		
	Equilibrium fuel moisture content (%)	as per (Kelley et al., 2014)	NCEP/NCAR relative humidity, temperature. (Kalnay et al., 1996)
			GPCP precipitation (monthly) (Adler et al., 2003)
	Tree Cover (%)		VCF (Dimiceli et al., 2015)
Potential ignitions “Ignitions” (no. km ⁻²)	Lightning strikes (strikes km ⁻²)	Cloud-to-ground as per (Kelley et al., 2014)	LIS/OTD lightning flash counts (Cecil et al., 2014)
	Population density (people km ⁻²)		HYDEv3.1 (Klein Goldewijk et al., 2010)
	Pasture (%)		
Anthropogenic suppression “Suppression”	Cropland (%)		
	Population density (people/km ²)		
Target	Burnt area		MCD64A1 burned area (Giglio et al., 2018)

Table S2: Driving data for optimization and simulation.

	July 2002 - June 2018	Jul 2019 - Jun 2020	Jul 2019 - Jan 2020
Land cover, land use, Population density	July 2002 - June 2018	July 2018 - Jun 2019	Jul 2018 - Jan 2020
All other variables	July 2002 - June 2018	Jul 2019 - Jun 2020	Jul 2019 - Jan 2020
Optimization	Used	Note used	
Simulation	Used		

145

150

References

- Adler, R. F., Huffman, G. J., Chang, A., Ferraro, R., Xie, P.-P., Janowiak, J., Rudolf, B., Schneider, U., Curtis, S., Bolvin, D., Gruber, A., Susskind, J., Arkin, P. and Nelkin, E.: The Version-2 Global
155 Precipitation Climatology Project (GPCP) Monthly Precipitation Analysis (1979–Present), *J. Hydrometeorol.*, 4(6), 1147–1167, 2003.
- Archibald, S., Roy, D. P., van WILGEN, B. W. and Scholes, R. J.: What limits fire? An examination of drivers of burnt area in Southern Africa, *Glob. Chang. Biol.*, 15(3), 613–630, 2009.
- Burton, C., Betts, R., Cardoso, M., Feldpausch, T. R., Harper, A., Jones, C. D., Kelley, D. I.,
160 Robertson, E. and Wiltshire, A.: Representation of fire, land-use change and vegetation dynamics in the Joint UK Land Environment Simulator vn4. 9 (JULES), *Geoscientific Model Development*, 12(1), 179–193, 2019.
- Cecil, D. J., Buechler, D. E. and Blakeslee, R. J.: Gridded lightning climatology from TRMM-LIS and OTD: Dataset description, *Atmos. Res.*, 135-136, 404–414, 2014.
- 165 Dimiceli, C., Carroll, M., Sohlberg, R., Kim, D. H., Kelly, M. and Townshend, J. R. G.: MOD44B MODIS/Terra Vegetation Continuous Fields Yearly L3 Global 250m SIN Grid V006, , doi:10.5067/MODIS/MOD44B.006, 2015.
- Dodge, Y.: Spearman rank correlation coefficient, *The Concise Encyclopedia of Statistics*. Springer, New York, 502–505, 2008.
- 170 Forkel, M., Carvalhais, N., Verbesselt, J., Mahecha, M. D., Neigh, C. S. R. and Reichstein, M.: Trend Change Detection in NDVI Time Series: Effects of Inter-Annual Variability and Methodology, *Remote Sensing*, 5(5), 2113–2144, 2013.
- Forkel, M., Migliavacca, M., Thonicke, K., Reichstein, M., Schaphoff, S., Weber, U. and Carvalhais, N.: Codominant water control on global interannual variability and trends in land surface phenology
175 and greenness, *Glob. Chang. Biol.*, 21(9), 3414–3435, 2015.
- Giglio, L., Boschetti, L., Roy, D. P., Humber, M. L. and Justice, C. O.: The Collection 6 MODIS burned area mapping algorithm and product, *Remote Sens. Environ.*, 217, 72–85, 2018.
- Hall, J. V., Loboda, T. V., Giglio, L. and McCarty, G. W.: A MODIS-based burned area assessment for Russian croplands: Mapping requirements and challenges, *Remote Sens. Environ.*, 184, 506–521,
180 2016.
- Hantson, S., Kelley, D. I., Arneth, A., Harrison, S. P., Archibald, S., Bachelet, D., Forrest, M., Hickler, T., Lasslop, G., Li, F., Mangeon, S., Melton, J. R., Nieradzki, L., Rabin, S. S., Colin Prentice, I., Sheehan, T., Sitch, S., Teckentrup, L., Voulgarakis, A. and Yue, C.: Quantitative assessment of fire and vegetation properties in historical simulations with fire-enabled vegetation models from the Fire
185 Model Intercomparison Project, *Geoscientific Model Development Discussions*, doi:10.5194/gmd-2019-261, 2020.
- Kalnay, E., Kanamitsu, M., Kistler, R., Collins, W., Deaven, D., Gandin, L., Iredell, M., Saha, S., White, G., Woollen, J., Zhu, Y., Chelliah, M., Ebisuzaki, W., Higgins, W., Janowiak, J., Mo, K. C., Ropelewski, C., Wang, J., Leetmaa, A., Reynolds, R., Jenne, R. and Joseph, D.: The NCEP/NCAR
190 40-Year Reanalysis Project, *Bull. Am. Meteorol. Soc.*, 77(3), 437–472, 1996.
- Kelley, D. I., Prentice, I. C., Harrison, S. P., Wang, H., Simard, M., Fisher, J. B., Willis, K. O. and

Others: A comprehensive benchmarking system for evaluating global vegetation models, [online]
Available from:
<https://www.researchonline.mq.edu.au/vital/access/services/Download/mq:26863/DS01>, 2013.

195 Kelley, D. I., Harrison, S. P. and Prentice, I. C.: Improved simulation of fire–vegetation interactions in the Land surface Processes and eXchanges dynamic global vegetation model (LPX-Mv1), *Geoscientific Model Development*, 7(5), 2411–2433, 2014.

Kelley, D. I., Bistinas, I., Whitley, R., Burton, C., Marthews, T. R. and Dong, N.: How contemporary bioclimatic and human controls change global fire regimes, *Nat. Clim. Chang.*, 9(9), 690–696, 2019.

200 Klein Goldewijk, K., Goldewijk, K. K., Beusen, A., Van Drecht, G. and De Vos, M.: The HYDE 3.1 spatially explicit database of human-induced global land-use change over the past 12,000 years, *Glob. Ecol. Biogeogr.*, 20(1), 73–86, 2010.

Lasslop, G., Moeller, T., D’Onofrio, D., Hantson, S. and Kloster, S.: Tropical climate–vegetation–fire relationships: multivariate evaluation of the land surface model JSBACH, *Biogeosciences*, 15(19),

205 5969–5989, 2018.

Rabin, S. S., Melton, J. R., Lasslop, G., Bachelet, D., Forrest, M., Hantson, S., Li, F., Mangeon, S., Yue, C., Arora, V. K. and Others: The Fire Modeling Intercomparison Project (FireMIP), phase 1: Experimental and analytical protocols, *Geoscientific Model Development*, 20, 1175–1197, 2017.

210

215